

Effects of respiratory rate on the fluid mechanics of a reconstructed upper airway

This is the author's version of a manuscript submitted for publication and accepted in the Journal: "Medical Engineering & Physics". Changes resulting from editing, structural formatting, and other final quality control mechanisms are not reflected in this document. For a final published version please see (Elsevier) : <https://doi.org/10.1016/j.medengphy.2021.103746>

Christopher Burchell¹, Agisilaos Kourmatzis^{2*}, Yongling Zhao³, Joel Raco¹, Taye Mekonnen¹

Hak-Kim Chan⁴, Shaokoon Cheng¹

* Corresponding author

1. School of Engineering, Macquarie University, Sydney, NSW, Australia

2. School of Aerospace, Mechanical and Mechatronic Engineering, University of Sydney

3. Department of Mechanical and Process Engineering, ETH Zürich, Zürich 8093, Switzerland

4. Sydney Pharmacy School, University of Sydney, Sydney, NSW, Australia

1 **Abstract:**

2 The effects of respiratory rate on the fluid dynamics present in the upper airway remain largely
3 uninvestigated. This study aims to utilise Particle Image Velocimetry (PIV) techniques to investigate the
4 time-dependent effects of respiratory rate in the extrathoracic airway, to show how they affect the flow
5 field developed. This is critical to validate and support the development of accurate airway flow
6 computational models. There has been limited validation of computational fluid dynamics (CFD) models
7 using experimental setups. Furthermore, the large majority of existing CFD models focus on rigid
8 airways, not accounting for active deformation through the breathing cycle. Experiments were carried
9 out using a transient, sinusoidal flow profile with two respiratory rates of 10 breaths per minute (BPM)
10 and 25 BPM, both achieving a maximum flow rate correlating to 5 L/min in air to simulate tidal
11 breathing. The flow was achieved using a piston pump to replicate the diaphragm's interaction with the
12 lungs, which was synchronised with active deformation of the model. Results from this study showed
13 that respiratory rate had the greatest influence near the onset of the inspiratory and expiratory
14 manoeuvres, with the higher respiratory rate homogenising later in the cycle. At the onset of inspiration,
15 the higher respiratory rate of 25 BPM only reached 15% of the peak flow of the 10 BPM case for the

16 rigid model and 48% for the actively deformed model. Additionally, it was shown that airway
17 deformation at the level of the soft palate homogenises flow downstream of the deformation which
18 results in a lower peak magnitude velocity for approximately 40% of the cycle at the level of the
19 epiglottis, when compared to the rigid airway model.

20 **Introduction**

21 Computational fluid dynamics (CFD) has been widely used to analyse and study the respiratory
22 airflow dynamics in the airways. These studies range from investigating flow behaviour after surgery of
23 the upper airway [1], studying the mechanisms by which sleep apnoea and treatment devices affect and
24 improve respiratory flow [2–5], to how the airway geometry influences flow and particle transport [6–
25 8]. Over the past decade, CFD has not only been used as a tool to shed light on airway pathology, its
26 usefulness as a surgical planning tool to improve respiratory flow has also been demonstrated [9]. CFD
27 studies of the upper airway have utilised both simple and complex, realistic airway geometries depending
28 on the focus of the studies. While a realistic airway geometry is necessary to inform details of flow
29 structures at specific anatomical regions of the pharynx, several studies have demonstrated that airway
30 geometry may be simplified depending on the goal of the study. Despite the advances made using both
31 realistic and simplified airway geometries, the majority of CFD models to date have been largely based
32 on the assumption of a rigid airway. In addition to this deficiency, there have also been limited
33 experimental studies conducted to investigate the flow field in the upper airway despite their unequivocal
34 importance towards validating the CFD models.

35 In recent years, there has been a growing interest to understand flow behaviour when the airway deforms
36 actively during respiration [10–12]. The first few studies conducted to investigate the effects of upper
37 airway deformation on airway flow were achieved by performing non-transient flow simulations in a
38 rigid airway model at the specific time point of the respiratory cycle [13]. A few other studies have also
39 modelled the airway as a tube which was allowed to deform through changes in the airway flow
40 [4,14,15]. While the afore-mentioned works shed light on how airflow-structure interaction can
41 potentially affect flow dynamics in the airway, detailed information of how physiologically realistic

42 deformation of the pharynx affects the fluid mechanics of the human upper airway remains sparse. The
43 human pharynx is formed by eight pharyngeal muscles whose functional integration is necessary to
44 perform complex tasks such as speech, swallowing, and breathing. Due to this function, certain sections
45 of the upper airway can actively widen during inspiration to promote airflow and not necessarily deform
46 and collapse, as would be observed in a conduit [16].

47 The realistic deformation of the upper airway and its dynamic effect on flow has recently been
48 demonstrated by Bate et al. [17,18] who simulated airflow in a CFD pharynx model with moving wall
49 boundaries. In the study, the magnitude of the soft tissue movement was obtained using fast-cine
50 magnetic resonance imaging (MRI). Results from the study show that considering airway movement
51 related to respiration can cause changes in pressure in the airway compared to rigid airway models. More
52 recently, Zhao et al. [19] performed the first experimental measurement using particle image velocimetry
53 (PIV) to show how active deformation of the pharynx (as observed in published MRI studies on pharynx
54 muscle contraction) affects fluid flow behaviour in the upper airway. Results show that the flow field is
55 significantly affected by wall movement and is in stark contrast with the results obtained using rigid
56 CFD models. The above-mentioned preliminary study, which only investigates a single flow case,
57 suggests the importance of considering the dynamic interaction between airway wall motion and air flow
58 when aiming to understand realistic flow dynamics in the extrathoracic airway. This is vital when the
59 goal is to produce clinically relevant computational models of respiratory airflow.

60 Many CFD studies have simulated constant flow. Naseri et al. [6] showed that steady-state flow and
61 transient flow simulation in a pharynx model resulted in notable differences in particle deposition
62 fraction in the airway. While the trends of deposition are the same for both the steady-state and transient
63 flow simulations, there are significant differences in the predicted mass of deposition, suggesting the
64 critical role of flow profile to achieve an accurate understanding of aerosol transport and deposition. In
65 a more recent study, Xu et al. [20] investigated the effects of three constant flow rates on upper airway
66 flow. The study shows that the flow rates affect the jet flow produced at the glottal region which was
67 less obvious in the experimental study produced by Zhao et al. [19], who simulated transient flow in a

68 actively deformed airway model. While changes in the pulsatility of biological fluid flow are common
69 in physiological processes, the effect of variability in this natural pulsatile behaviour has rarely been
70 addressed and studied systematically [21, 23] in the context of respiratory rate and upper airway flow.

71 This study aims to elucidate the effects of airflow pulsatility (respiratory rate) in both a rigid and an
72 actively deformed, geometrically realistic, extrathoracic airway model using PIV. Specifically, the
73 effects of frequency of tidal breathing will be investigated, with a secondary emphasis on the influence
74 of the model deformation and the transient flow profile. This is critical to validate and support the
75 development of accurate airway flow computational models.

76 **Methods**

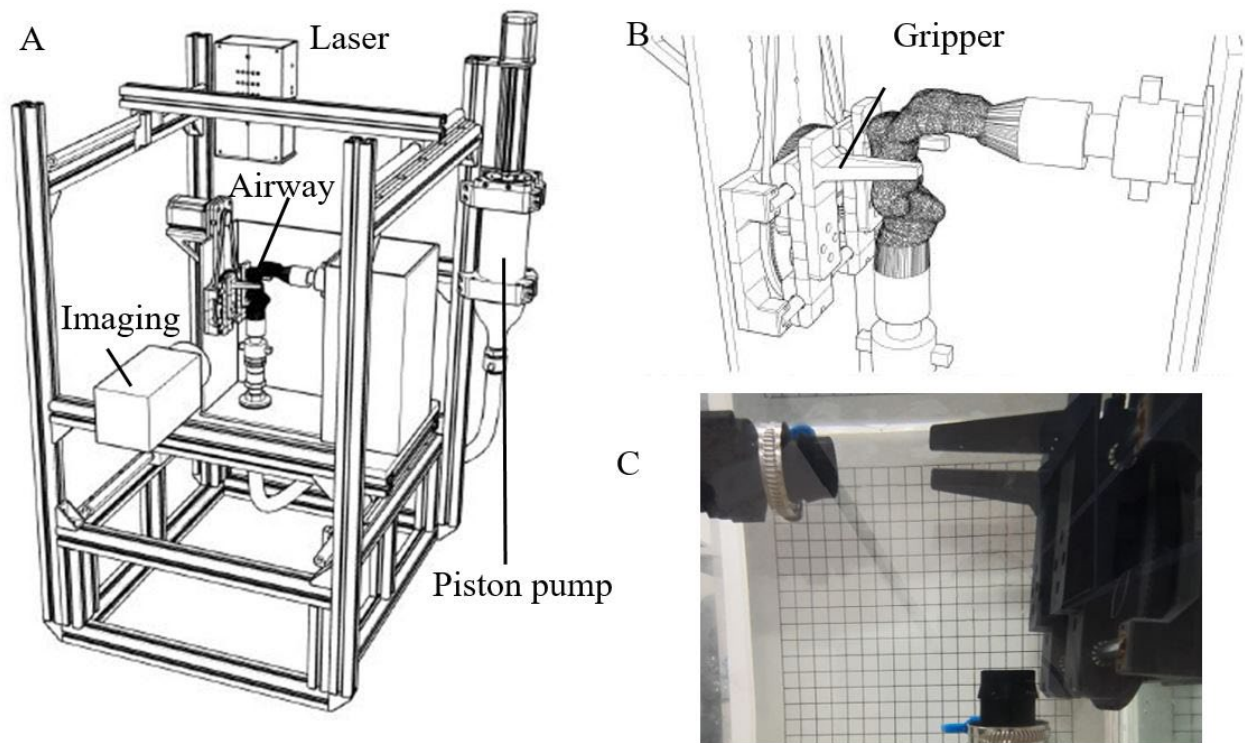
77 *Silicone Phantom*

78 MRI data were collected from a healthy middle-aged female with a body mass index (BMI) of 20 kg/m².
79 The upper airway was reconstructed using open source software 3D Slicer (www.slicer.org, [22]). The
80 airway geometry was scaled to 1.5 times its original dimensions to allow for increased optical access. A
81 three-piece mould; consisting of two halves and one sacrificial, was designed using Rhinoceros 3D
82 (www.rhino3d.com) such that the airway geometry could be cast in optically transparent silicone rubber
83 with specific wall thickness. A wall thickness of 3 millimetres was used because preliminary studies
84 have been performed to ensure that the induced flow passing through the silicone phantom was unable
85 to distort the airway geometry with this wall thickness, while still allowing the mechanical gripper to
86 deform the airway at the desired regions. The mould was manufactured using rapid prototyping
87 technologies and post-processed to create a smooth surface finish while at the same time ensuring optical
88 accessibility. After casting, the two halves were removed and the sacrificial piece dissolved, leaving
89 behind the silicone phantom. The model was connected to the rest of the flow system using rigid fittings,
90 these were calculated to present a homogenous flow for the inflow and outflow conditions of the model.

91 *Particle image velocimetry setup*

92 An overall view of the setup is presented in Figure 1. A piston pump controlled by an actuator provided

93 a controllable flow rate vs. time profile and acted as a diaphragm pushing and pulling fluid through the
94 silicone phantom to simulate tidal breathing. A mechanical gripper was positioned at the bottom of the
95 uvula, slightly below the soft palate, simulating the deformation of the airway lateral walls that has been
96 observed at this level of the pharynx in published MRI studies (Figure 1-C) [10,11,23]. The mechanical
97 gripper was also synchronised with the piston pump, which triggered the PIV laser and cameras. Both
98 the actuator and gripper were powered by Nema 23 stepper motors, allowing the pump to deliver a flow
99 that represents 5 L/min of air and achieving a resolution of 0.038s. The refractive index of the silicone
100 material used to fabricate the complex airway geometry was matched with glycerol by submerging the
101 phantom in a water glycerol mixture of 44 parts water to 56 parts glycerol by weight, resulting in a
102 kinematic viscosity of $5.96 \times 10^{-6} \text{ m}^2/\text{s}$ and a density of 1138 Kg/m^3 . The tracer particles used were
103 refractive glass spheres with a mean size of 9 to 13 micrometres from MilliporeSigma (www.MilliporeSigma.com)
104 were used to seed the fluid within the airway model such that approximately 5 –
105 10 particles were present in each interrogation window of cross-correlation. A double pulsed Nd:YAG
106 laser (Evergreen) was used with a camera exposure time of 25us and an interframe time of 250us. The
107 laser sheet was approximately 0.7mm, the pco camera utilised an EF 50mm 1:1.4 lens. The camera was
108 positioned approximately 250mm away from the laser sheet. The setup produced images with a spatial
109 resolution of 1600 pixel x 1200 pixel, with a FOV of 50mm x 37.5mm. The interrogation window size
110 was set to 128 pixels x 128 pixels with a 50% overlap. Digital cross correlation was used to determine
111 the displacement of particles. Post-processing of particle images adopted similar methods reported in
112 Zhao et al. [19].

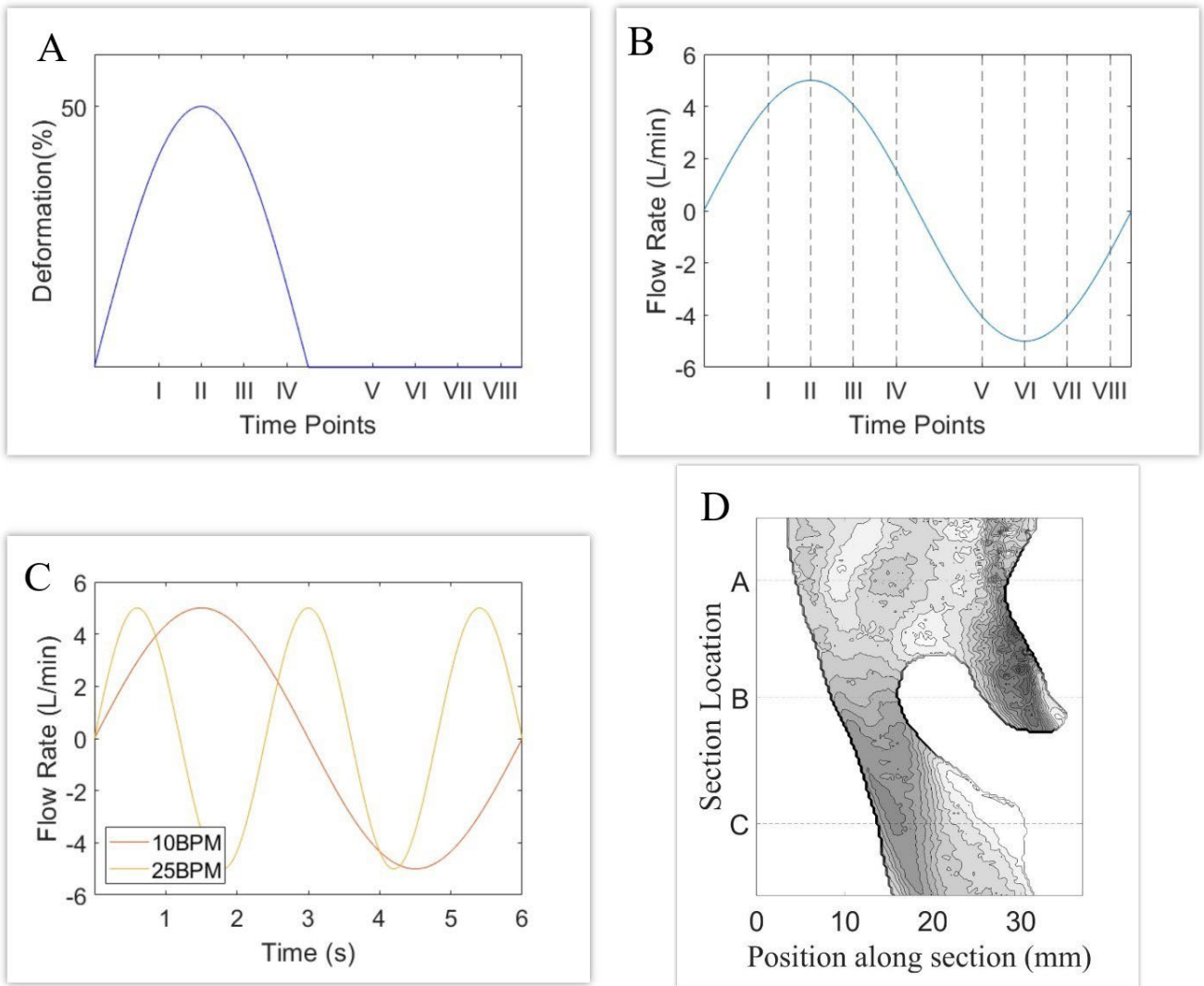


113
 114
 115 *Figure 1. A) The panel shows the PIV setup. The airway is placed in a glass tank connected to a piston pump and reservoir. Laser sheet*
 116 *is projected downwards along the centre of the silicone phantoms in the sagittal plane. Imaging camera is located perpendicular to the*
 117 *laser sheet and focused on the epiglottis and surrounding regions. B) Close up view of the airway gripper used to simulate upper airway*
 118 *deformation. The gripper utilises two arms which extends beyond the anterior end of the airway geometry. C) Panel shows the side view*
 119 *of the experimental setup and the undistorted grid (placed behind the airway) shows that optical distortion has been adequately resolved.*

120 *Data Collection*

121 A sinusoidal breathing profile with an equivalent peak flow rate of 5 L/min of air was simulated in this
 122 study. The frequency of breathing simulated was 10 and 25 breaths per minute, taken from a study
 123 recording respiratory rates in the population [24]. Both the Reynolds number and Womersley number
 124 were matched in the experiments, allowing for the recreation of the flow characteristics present in air in
 125 the greater viscosity working fluid of the glycerol mixture. The Reynolds number is defined as a
 126 dimensionless number that characterises the ratio between inertial forces and viscous forces. The
 127 Womersley number is a dimensionless expression of the relation between pulsatile flow frequency and
 128 viscous effects. The maximum Reynolds calculated was 425 and the Womersley number of the 10 BPM
 129 and 25 BPM cases was 1.74 and 2.75 respectively. The Reynolds number was calculated using a length-
 130 scale which was measured from the MRI image as the smallest diameter at the smallest cross section,
 131 which was located near the epiglottis. The mean maximum velocity was calculated from the maximum
 132 flow rate of 5 L/min in relation to the cross-sectional area at the same point. The same length-scale was

133 used in the calculation of the Womersley number. Preliminary studies were performed to determine that
134 20 imaging repetitions of instantaneous velocity fields on a phase locked loop were sufficient to
135 reproduce the flow pattern accurately for all breathing frequencies. The flow was imaged along the mid-
136 sagittal plane of the airway, as the model isnt perfectly symmetrical, this was chosen as a line of best fit
137 along the rear wall of the airway, taking the lateral ends of the airway and bisecting for the mid points.
138 The flow field in the airway, as a function of breathing frequency, was obtained in a rigid and in a
139 actively deformed airway. In the experiment on the deformed airway, a predetermined deformation was
140 simulated, using the gripper such that the airway was narrowed laterally by half its maximum width at
141 peak inspiration [11,19]. Figure 2 shows the flow rate, airway deformation profile and the time points
142 chosen for discussion in this study. The time points were chosen to illucidate the trends over the entirety
143 of the cycle, the transistion between inspiration and expiration was exluded due to lack of difference
144 between flow profiles. Unless otherwise stated, when referring to mean velocities in the Results section,
145 reference is being made to the mean velocity in the vertical (y) direction.



146
147
148
149
150
151
152

Figure 2. Eight time points (TP) have been selected for discussion and they are represented by grey vertical lines in Panel A and B. A) Deformation profile. The airway was deformed laterally by 50% of its width and no deformation was simulated during expiration. B) Panel shows the sinusoidal flow rate profile in which the positive flow rate corresponds to inspiration. C) Flow profile for 10BPM and 25BPM. Time in X-axis is not the same as the time point described in panel A and B. D) Panel shows the three locations (section A, B and C) where the velocity profiles are analysed.

153 **Results**

154 (i) *Flow field description (Figure 3) - the difference between a rigid and actively deformed*
155 *airway*

156 Time Point I –Beginning of Inspiration

157 At TP I, results show that the change in breathing frequency affects the mean flow field in both the rigid
158 and actively deformed airways (See Figure 3). At 10 BPM, the flow field above the epiglottis (see the
159 location of epiglottis highlighted as a black boundary line in Figure 2D), in the actively deformed

160 airway, is more posteriorly directed (white arrow) demonstrating the apparent effects of lateral airway
161 wall deformation at the soft palate. The velocity magnitude at the narrowest region of the airway
162 (adjacent to the epiglottis tip; next to the red arrow) is also higher in the rigid airway. At 25 BPM, the
163 highest velocity magnitudes in the rigid and actively deformed airway models are less than 25% of the
164 magnitude of the 10 BPM results.

165 Time Point II

166 At TP II, both the rigid and actively deformed airway are affected by the breathing frequency such that
167 the velocity magnitude is much lower at the narrowest region of the airway for the 25BPM cases. While
168 there is a more concentrated jet-like flow behind the tongue [25] and adjacent to the epiglottis in the
169 rigid airway at 10 BPM, these flow fields are not observed in the actively deformed airway,
170 demonstrating that the lateral deformation of the airway at the soft palate has the effect of homogenising
171 flow.

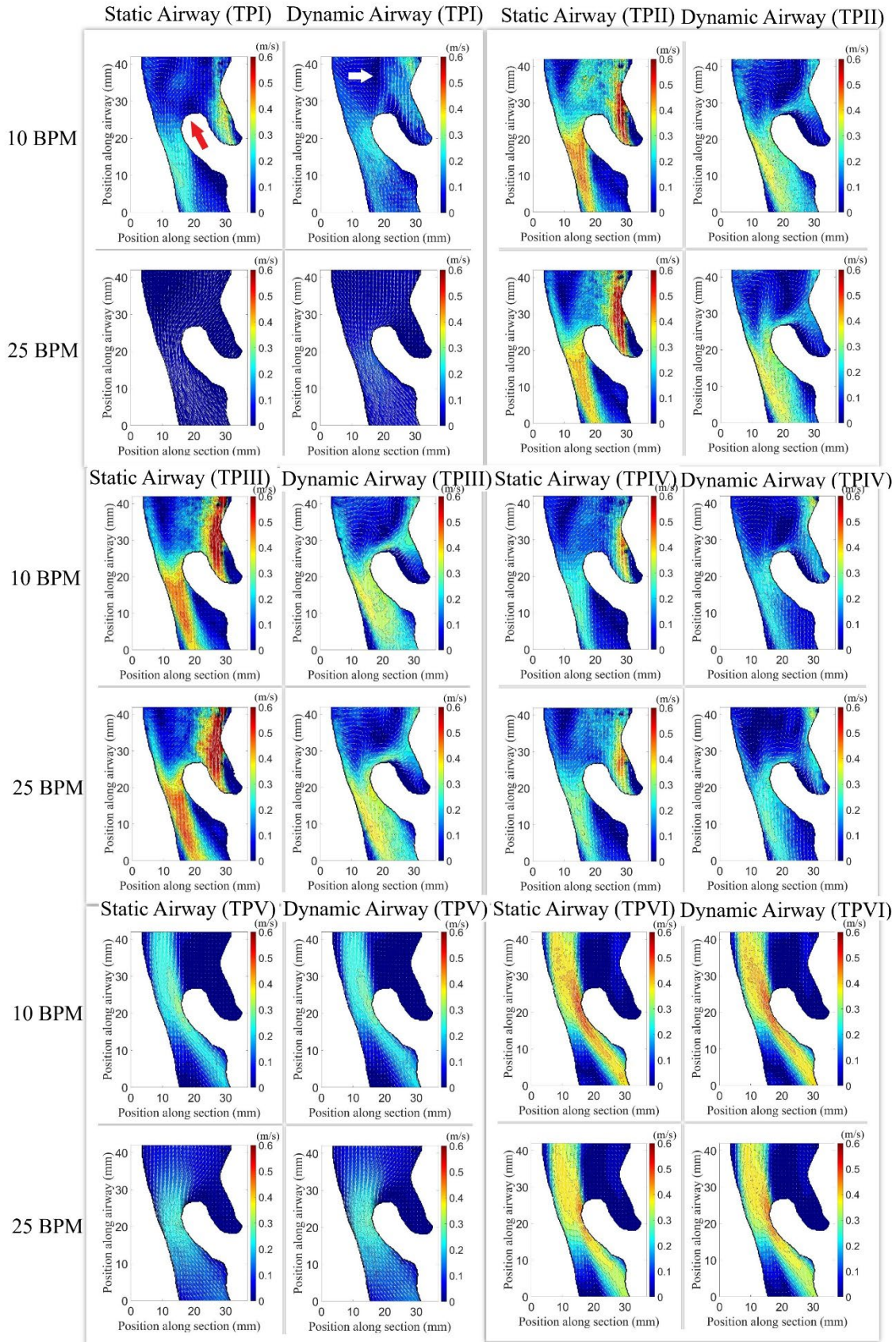
172 Time Point III & IV

173 At TP III, the effects of breathing frequency on the flow dynamics diminish in both the rigid and actively
174 deformed airway, although there is a distinctive difference between the flow field developed in the rigid
175 and actively deformed airway models. For example, while horizontal and posteriorly directed flow
176 vectors are evident in the actively deformed airways, they are absent in the rigid airways. Breathing
177 frequency appears to have no obvious effect on the flow field generated in the airways at TP IV but
178 noticeable differences in results between the rigid and actively deformed airways can be observed (as
179 with TP III). For example, the jet-like flow at the narrowest section of the airway is less apparent in the
180 actively deformed airway model compared to the rigid airway model.

181 Time Point V & VI- Expiration

182 TP V occurs during the expiratory phase. At this time point, some differences between the flow fields
183 developed at 10 BPM and 25 BPM can be observed for both the rigid and actively deformed airways.
184 There is an extended high-velocity flow region at the narrowest section of the airway (see the region in

185 the rectangular inset) in the cranial caudal (up – down) direction for the models at 10 BPM. The flow
186 velocity directly above the tip of the epiglottis (see the region in the circular inset) is also higher in the
187 models with higher breathing frequency. There are no observable differences between the rigid and
188 actively deformed airway models, which is expected due to the lack of active deformation in the
189 expiration manoeuvre. At TP V, it is clear that the frequency of the pulsatile flow has a noticeable effect
190 on the flow field in the airway models. During the second time point of the expiratory phase (TP VI),
191 for the 10 BPM case, there is a higher velocity magnitude at the narrowest region of the airway (adjacent
192 to the epiglottis), than evident on the 25 BPM cases. This is likely due to the higher fluid acceleration
193 found in the 25 BPM cycle, causing higher flow concentration with less homogenisation. The flow field
194 in the rigid and actively deformed airway models are similar. As the flow field measurements were taken
195 independently in the rigid and actively deformed airway models, the results presented, therefore also
196 demonstrate the repeatability of the PIV measurements.



197
198
199
200

Figure 3. Velocity flow field at different time points during inspiration. Panel shows the flow field differences caused by breathing frequency and also airway deformation. The velocity magnitude (m/s) is presented in the coloured scale on the right.

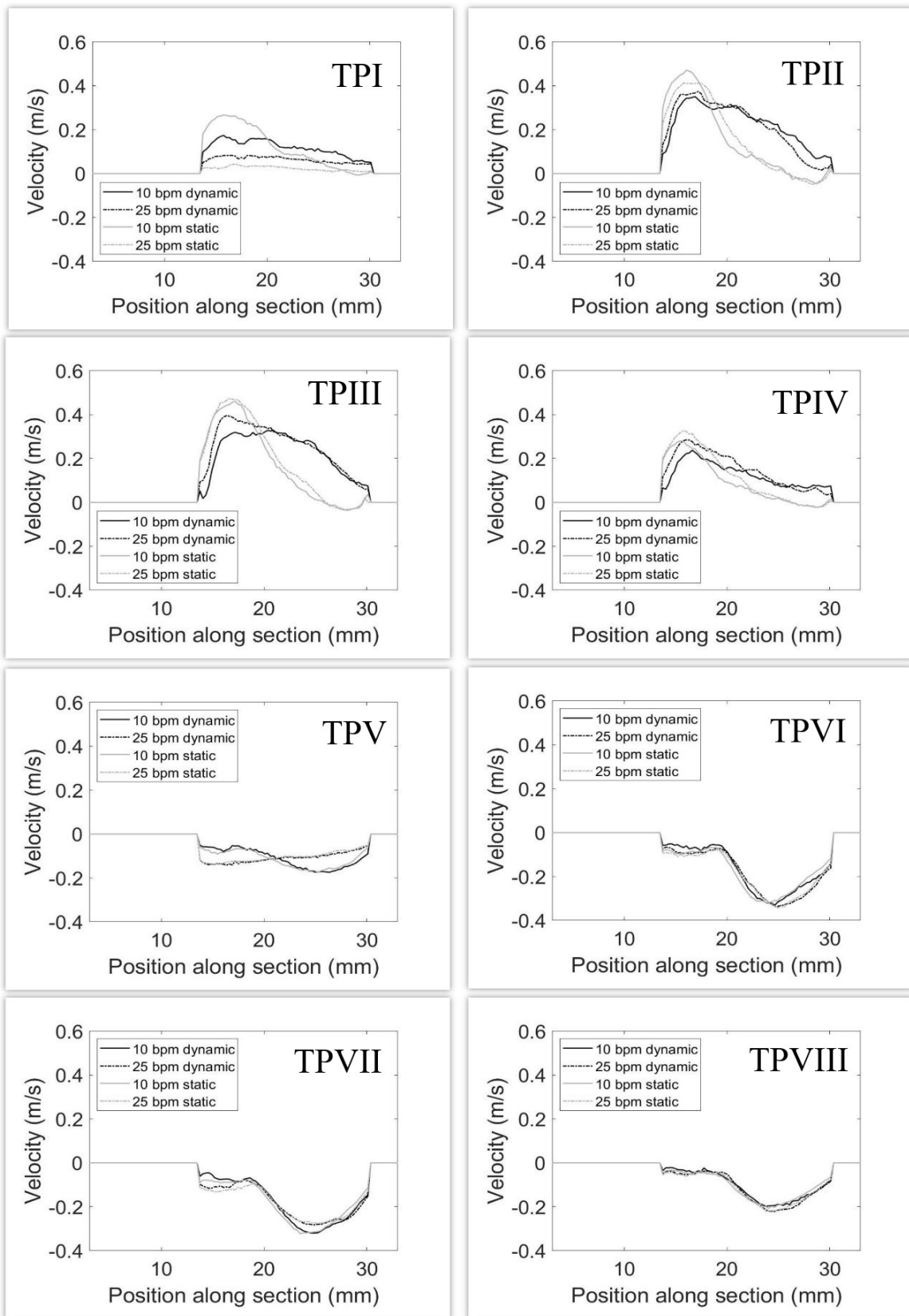
201 (ii) Velocity flow profile. (Figure 4 & 5)

202 Frequency of breathing appears to affect the velocity profile (velocity in y direction vs. distance
203 across lumen cross section) during the early phase of inspiration and expiration, and the effect seems to
204 be more apparent in the rigid airway compared to the actively deformed airway. Figure 4 shows the
205 velocity profile in the y direction across the breadth of the lumen through section C, recorded at the
206 various time-points throughout the respiratory cycle (see Figure 2), and there are a number of
207 observations. Firstly, the velocity profile is usually different between the rigid (grey coloured lines) and
208 actively deformed airway model (black coloured lines), highlighting the potential effects of airway wall
209 deformation. In particular for time points I, II and III, there is a very distinctive difference in the profiles,
210 with the actively deformed airway models showing a much broader velocity distribution, compared to
211 the rigid which has a concentrated region of higher velocity, followed by a steep decline. The steep
212 decline is also followed by a longer region of near stagnant fluid, from a position of 26 to 30 mm. Apart
213 from timepoint I, this fundamental difference in the velocity profile shape seems to be largely unaffected
214 by the frequency of breathing. At the transition to inspiration there is a large difference in the profiles
215 for the different respiratory rates again, which is more pronounced in the rigid model than the actively
216 deformed model. The 25 BPM case in the rigid model only achieves approximately 15% of the peak
217 flow of the 10 BPM case. This relationship is again expressed in the actively deformed model, but to a
218 less extensive degree, with the 25 BPM case only achieving a peak flow of approximately 48% of the
219 peak flow recorded in the 10 BPM case.

220 As the transition to the expiratory phase occurs, at time Point V the differences observed between
221 the actively deformed and rigid models diminish significantly, however an effect of the breathing
222 frequency is noted. This effect showed an anterior flow concentration for the 10 BPM case and a more
223 posterior flow concentration for the higher frequency, 25 BPM case. It is particularly interesting how
224 both the actively deformed and rigid airway models exhibit the same change in velocity profile when
225 moving from 10 to 25 BPM, with almost no discernible difference in the velocity profile as a function
226 of dynamic wall motion. After this transitional time point, there is no active deformation, as such it was
227 expected that there would be no difference due to the effect of airway wall motion. Interestingly, there

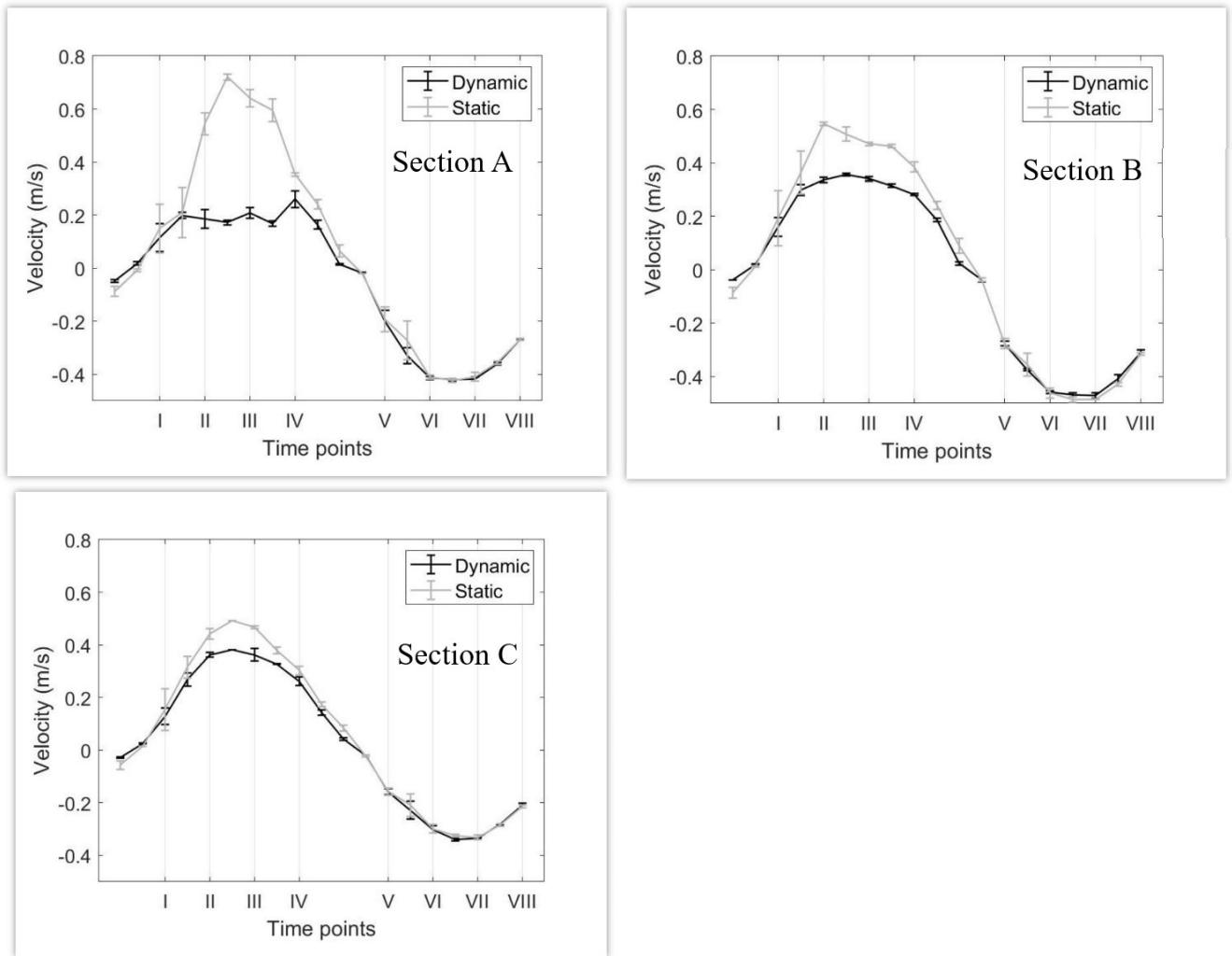
228 is also no discernible effect from the breathing frequency through the majority of the expiratory half of
229 the cycle.

230 Figure 5 shows the maximum vertical velocity, averaged over 20 repeat cycles, for the flow
231 profiles of the 10 and 25 BPMs collected at different time points of the respiratory cycle. The data is
232 presented for each specified time point, gathered along the three identified sections (A, B and C). The
233 peak velocity is consistently higher in the rigid airway model than the actively deformed airway for all
234 time points before expiration commences. The results show that the difference in maximum velocity
235 between the actively deformed and rigid airways can be as high as 26%. With airway deformation above
236 the epiglottis, absence of flow through the piriform sinuses can be found, this is highlighted by the high
237 anterior flow through section A of the rigid airway in which there is higher adhesion to the rear of the
238 tongue. The standard deviation from figure 5 is recorded by taking the maximum vertical velocity from
239 each time point, averaged over twenty repeat cycles, as the population values, then averaging across both
240 BPM values. The standard deviation is then calculated using standard equations between the maximum
241 values against the average. As such, the standard deviations in the figures can be used to infer the effects
242 associated with underlying differences in breathing frequency, and would also be an indicator of the
243 degree of underlying fluctuations or intermittency in the flow, it could also indicate a change in greater
244 out of plane motion. The magnitude of the error bars suggests that a rigid airway is more susceptible to
245 breathing frequency and that a actively deformed airway has the effects of reducing maximum velocity
246 for flow profiles downstream of the airway from where the airway deforms.



247
248
249
250

Figure 4. Comparison of velocity flow profile at section C between the static and dynamic airway models for breathing frequencies 10 and 25 BPM.



251
252
253

Figure 5. Average maximum velocity for measurements taken at 10 and 25 BPMs at section A, B and C.

254 **Discussion**

255 To the best of the author’s knowledge, this is the first experimental research study performed to
 256 understand the effects of respiratory flow pulsatility developed in a rigid
 257 and actively deformed extrathoracic airway. According to studies performed using MRI [12], the
 258 patterns of upper airway deformation can be different between individuals, and they are related to the
 259 combined effects of passive and active deformation of the airway, where the latter is caused by
 260 contraction of the upper airway muscles during respiration. This model is based on the images of a
 261 singular individual, with an airway diameter below the 50th percentile for the available geometries. This
 262 has resulted in a relatively low Reynolds number when modelling tidal breathing, this is due to the
 263 necessity of thin walls for the model to emulate the deformation patterns evident in the upper airways.
 264 When higher flow rates are modelled, passive deformation, which isn’t representative of airway

265 deformation occurs. Furthermore, this is using generated flow profiles, as such these results may vary
266 between different models with different geometries.

267

268 A flexible airway model is unlikely to accurately replicate the actual deformation pattern of the pharynx
269 in humans, especially when the soft tissues surrounding the upper airway in the airway models are only
270 represented by a structure with uniform wall thickness. Subsequently, the collapse of airway model
271 replicas is unlikely to emulate physiologically realistic flow field in the airway. This is because
272 representing the pharynx boundaries using flexible membrane structure with uniform thickness will not
273 meaningfully emulate the heterogeneous mechanical properties and bulk soft tissue structures that
274 surround the pharynx [26].

275 The main finding from this study is that breathing frequency affects the flow field distinctively
276 in both the rigid and actively deformed airway models with the most dramatic effect occurring before
277 peak inspiratory flow (Time point II). The principal mechanism for the changes in the velocity flow field
278 as a function of breathing frequency is primarily related to the differences in fluid mass entering the
279 airway in a given period. The magnitude of peak flow rate was maintained throughout the study in order
280 to provide a meaningful comparison on the effects that are solely caused by breathing frequency. While
281 this study doesn't have any steady state flow conditions, they would be important for future validation.
282 The volume of fluid that enters the airway decreases with the increase in breathing frequency, which
283 resulted in a higher acceleration rate and higher average velocity in the mid sagittal plane of the airway.
284 This was evident at the onset of inspiration and expiration. At time point I, there was largely reduced fluid
285 flow through the midsagittal plane for the higher frequency models. There are a number of potential
286 causes for this effect. Firstly, it is important to note that the measurements do not account for the flows
287 external to the measured plane (midsagittal) and an additional study imaging the 3d flow field would be
288 highly valuable, although this isn't within the scope of the current work. Additionally, the laser plane
289 used, in combination with standard PIV as opposed to Stereo PIV, may lead to a higher perspective
290 error. As the flow rate is the same for each compared time point between the breathing frequencies, the

291 measured velocity field of lower value indicates alternate flow paths external to the midsagittal due to
292 mass conservation of the flow. Due to this effect being more pronounced at the onset of the cycles, it is
293 likely that residual flow is having an effect. This would explain why the higher frequency cycle (25
294 BPM), which had less time to stabilise the flow, exhibited more pronounced effects when changing from
295 expiration to inspiration or visa versa. Furthermore the rigid model, without the active deformation of
296 the airway, took longer to stabilise flow field as evidenced by the less homogenous flow in figures 3 and
297 4. The effects of respiratory rate became less pronounced as the cycle reached peak flows, where the flow
298 was stabilised.

299 Although the first insights of airway deformation and their effects on the velocity flow field
300 developed in the airway have been addressed[19], overview of the velocity flow field in a geometrically
301 realistic and actively deformed airway replica has not been demonstrated for a complete respiratory cycle
302 and the results are reported in this current study. It is important to note that as these measurements are
303 planar, they don't account for out of plane flow, which may contribute to any errors or standard
304 deviations. Findings from this study provide further evidence that airway deformation at the level of the
305 soft palate [12,23] has the effect of homogenising flow downstream of the location where the airway
306 deforms. Deformation of the airway also results in a lower peak velocity magnitude compared to the
307 rigid airway models. In fact, the maximum velocity at the level of the airway above the epiglottis is
308 significantly lower in the actively deformed airway compared to the rigid airway for ~ 40% of the
309 respiratory cycle and before peak inspiration occurs. Interestingly, in the actively deformed airway
310 model, the average maximum velocity appears to be less affected by changes in breathing frequency.

311 The velocity flow field demonstrated in this current study is important and useful to validate the
312 accuracy of CFD models that simulate air flow in the pharynx. The cross sectional areas of the upper
313 airway model were consistent with what had been found in other physiological studies [27]. The
314 velocities found in the imaging were consistent with what had been calculated using the input flow rate
315 and the correlating cross sectional area. A general finding in published CFD work of upper airway flow,
316 which also typically simulates constant flow rate [20,25] is the presence of a jet flow at the posterior

317 wall of the pharynx downstream of the epiglottis during inhalation.

318 This has been verified further through other CFD studies at similar low, transient flow
319 rates [18,28,29]. For further validation, clinical data of flow characteristics present in low flow rates
320 needs to be gathered. Vital anatomical features that are commonly missing in the replicas used in
321 previous work include the uvula, the piriform sinuses, and a fully protruding epiglottis. Results from this
322 current study show that the epiglottis and piriform sinuses result in a highly concentrated flow region at
323 the back of the tongue and the effect dissipates with airway wall deformation at the level of the soft
324 palate. In fact, deformation of the upper airway results in a distinctly different flow field as it
325 homogenises flow downstream of the deformation location and generates horizontal and posteriorly
326 directed flow (towards the back of the tongue) before peak inspiration occurs.

327 **Conclusion**

328 Despite the decades of intensive research on airway flow mechanics, there is very limited
329 experimental work for the validation of CFD models. This is despite the fact that both experimental
330 studies and simulations are complementary and play important roles in accomplishing the overarching
331 goal to improve the knowledge of airway flow dynamics. There is wide application of knowledge in
332 upper airway flows, and advancement in this field can continue to benefit from in-depth understanding
333 of upper airway physiology. At the flow-rates examined here, findings from the study indicate that
334 respiratory rate only has an impact without the presence of active deformation. The flow profiles for
335 both frequencies showed similar trends when combined with active deformation, with the main
336 differences emerging only between rigid model cases. This highlights the importance of including wall
337 movement in airways when modelling particle flow, and furthermore, it may have implications for both
338 sleep apnoea and mechanical ventilation of unconscious patients, where there is reduced upper airway
339 muscle activation. This current study, together with a few recent works, have unveiled new
340 information on flow dynamics which have been previously overlooked. Further
341 research on physiologically realistic airway flow is necessary to improve our
342 understanding of respiratory mechanics in health and disease.

343 **Acknowledgements**

344 Conflicts of interest: None declared.

345 Funding: Funding for this publication was made possible, in part, by the Australian Research Council,
346 Australia through grant DP190101237 and the Food & Drug Administration (United States) through
347 grant 1U01FD006525 - 01.

348 Views expressed do not necessarily reflect the official policies of the Department of Health and
349 Human Services; nor does any mention of trade names, commercial practices, or organization imply
350 endorsement by the United States Government.

351 The first author is funded by a PhD scholarship from the Australian Government Research Training
352 Program.

353 Ethical Approval: Not required.

Bibliography

- [1] Zhu L, Liu H, Fu Z, Yin J. Computational fluid dynamics analysis of Huvulopalatopharyngoplasty in obstructive sleep apnea syndrome. *Am J Otolaryngol - Head Neck Med Surg* 2019;40:197–204. <https://doi.org/10.1016/j.amjoto.2018.12.001>.
- [2] Li L, Wu W, Yan G, Liu L, Liu H, Li G, et al. Analogue simulation of pharyngeal airflow response to Twin Block treatment in growing patients with Class II 1 and mandibular retrognathia. *Sci Rep* 2016;6:1–7. <https://doi.org/10.1038/srep26012>.
- [3] Kim T, Kim HH, Hong SO, Baek SH, Kim KW, Suh SH, et al. Change in the upper airway of patients with obstructive sleep apnea syndrome using computational fluid dynamics analysis: Conventional maxillomandibular advancement versus modified maxillomandibular advancement with anterior segmental setback osteotomy. *J Craniofac Surg* 2015;26:e765–70. <https://doi.org/10.1097/SCS.0000000000002209>.
- [4] Zhao M, Barber T, Cistulli P, Sutherland K, Rosengarten G. Computational fluid dynamics for

the assessment of upper airway response to oral appliance treatment in obstructive sleep apnea. *J Biomech* 2013. <https://doi.org/10.1016/j.jbiomech.2012.10.033>.

- [5] Song B, Li Y, Sun J, Qi Y, Li P, Li Y, et al. Computational fluid dynamics simulation of changes in the morphology and airflow dynamics of the upper airways in OSAHS patients after treatment with oral appliances. *PLoS One* 2019;14:e0219642. <https://doi.org/10.1371/journal.pone.0219642>.
- [6] Naseri A, Shaghaghian S, Abouali O, Ahmadi G. Numerical investigation of transient transport and deposition of microparticles under unsteady inspiratory flow in human upper airways. *Respir Physiol Neurobiol* 2017;244:56–72. <https://doi.org/10.1016/j.resp.2017.06.005>.
- [7] Rahiminejad M, Haghghi A, Dastan A, Abouali O, Farid M, Ahmadi G. Computer simulations of pressure and velocity fields in a human upper airway during sneezing. *Comput Biol Med* 2016;71:115–27. <https://doi.org/10.1016/j.compbimed.2016.01.022>.
- [8] Islam MS, Saha SC, Gemci T, Yang IA, Sauret E, Ristovski Z, et al. Euler-Lagrange Prediction of Diesel-Exhaust Polydisperse Particle Transport and Deposition in Lung: Anatomy and Turbulence Effects. *Sci Rep* 2019;9:1–16. <https://doi.org/10.1038/s41598-019-48753-6>.
- [9] Clipp RB, Vicory J, Horvath S, Mitran S, Kimbell JS, Rhee JS, et al. An Interactive, Patient-Specific Virtual Surgical Planning System for Upper Airway Obstruction Treatments. *Conf Proc . Annu Int Conf IEEE Eng Med Biol Soc IEEE Eng Med Biol Soc Annu Conf* 2018;2018:5802–5. <https://doi.org/10.1109/EMBC.2018.8513672>.
- [10] Cheng S, Butler JE, Gandevia SC, Bilston LE. Movement of the tongue during normal breathing in awake healthy humans. *J Physiol* 2008;586:4283–94. <https://doi.org/10.1113/jphysiol.2008.156430>.
- [11] Cheng S, Kourmatzis A, Mekonnen T, Gholizadeh H, Raco J, Chen L, et al. Does Upper Airway Deformation Affect Drug Deposition? *Int J Pharm* 2019:118773.

<https://doi.org/10.1016/j.ijpharm.2019.118773>.

- [12] Cheng S, Butler JE, Gandevia SC, Bilston LE. Movement of the human upper airway during inspiration with and without inspiratory resistive loading. *J Appl Physiol* 2011;110:69–75. <https://doi.org/10.1152/jappphysiol.00413.2010>.
- [13] Yin Y, Choi J, Hoffman EA, Tawhai MH, Lin CL. A multiscale MDCT image-based breathing lung model with time-varying regional ventilation. *J Comput Phys* 2013. <https://doi.org/10.1016/j.jcp.2012.12.007>.
- [14] Zhu JH, Lee HP, Lim KM, Lee SJ, Teo LSL, Wang DY. Passive movement of human soft palate during respiration: A simulation of 3D fluid/structure interaction. *J Biomech* 2012. <https://doi.org/10.1016/j.jbiomech.2012.04.027>.
- [15] Wang Y, Wang J, Liu Y, Yu S, Sun X, Li S, et al. Fluid-structure interaction modeling of upper airways before and after nasal surgery for obstructive sleep apnea. *Int j Numer Method Biomed Eng* 2012. <https://doi.org/10.1002/cnm.1486>.
- [16] Cheng S, Brown EC, Hatt A, Butler JE, Gandevia SC, Bilston LE. Healthy humans with a narrow upper airway maintain patency during quiet breathing by dilating the airway during inspiration. *J Physiol* 2014. <https://doi.org/10.1113/jphysiol.2014.279240>.
- [17] Bates AJ, Schuh A, Amine-Eddine G, McConnell K, Loew W, Fleck RJ, et al. Assessing the relationship between movement and airflow in the upper airway using computational fluid dynamics with motion determined from magnetic resonance imaging. *Clin Biomech* 2019;66:88–96. <https://doi.org/10.1016/j.clinbiomech.2017.10.011>.
- [18] Bates AJ, Schuh A, McConnell K, Williams BM, Lanier JM, Willmering MM, et al. A novel method to generate dynamic boundary conditions for airway CFD by mapping upper airway movement with non-rigid registration of dynamic and static MRI. *Int j Numer Method Biomed Eng* 2018;34:1–19. <https://doi.org/10.1002/cnm.3144>.

- [19] Zhao Y, Raco J, Kourmatzis A, Diasinos S, Chan H-K, Yang R, et al. The effects of upper airway tissue motion on airflow dynamics. *J Biomech* 2020;99:109506. <https://doi.org/10.1016/j.jbiomech.2019.109506>.
- [20] Xu X, Wu J, Weng W, Fu M. Investigation of inhalation and exhalation flow pattern in a realistic human upper airway model by PIV experiments and CFD simulations. *Biomech Model Mechanobiol* 2020. <https://doi.org/10.1007/s10237-020-01299-3>.
- [21] Le TB, Borazjani I, Sotiropoulos F. Pulsatile flow effects on the hemodynamics of intracranial aneurysms. *J Biomech Eng* 2010. <https://doi.org/10.1115/1.4002702>.
- [22] Fedorov A, Beichel R, Kalpathy-Cramer J, Finet J, Fillion-Robin JC, Pujol S, et al. 3D Slicer as an image computing platform for the Quantitative Imaging Network. *Magn Reson Imaging* 2012. <https://doi.org/10.1016/j.mri.2012.05.001>.
- [23] Trudo FJ, Geftter WB, Welch KC, Gupta KB, Maislin G, Schwab RJ. State-related changes in upper airway caliber and surrounding soft-tissue structures in normal subjects. *Am J Respir Crit Care Med* 1998. <https://doi.org/10.1164/ajrccm.158.4.9712063>.
- [24] Addison PS, Watson JN, Mestek ML, Mecca RS. Developing an algorithm for pulse oximetry derived respiratory rate (RRoxi): A healthy volunteer study. *J Clin Monit Comput* 2012. <https://doi.org/10.1007/s10877-011-9332-y>.
- [25] Ma B, Kourmatzis A, Zhao Y, Yang R, Chan HK, Salehi F, et al. Potential effects of lingual fats on airway flow dynamics and particle deposition. *Aerosol Sci Technol* 2019. <https://doi.org/10.1080/02786826.2019.1696014>.
- [26] Cheng S, Gandevia SC, Green M, Sinkus R, Bilston LE. Viscoelastic properties of the tongue and soft palate using MR elastography. *J Biomech* 2011;44:450–4. <https://doi.org/10.1016/j.jbiomech.2010.09.027>.
- [27] Chousangstorn K, Bhongmakapat T, Apirakkittikul N, Sungkarat W, Supakul N, Laothamatas

J. Upper Airway Areas, Volumes, and Linear Measurements Determined on Computed Tomography During Different Phases of Respiration Predict the Presence of Severe Obstructive Sleep Apnea. *J Oral Maxillofac Surg* 2018;76:1524–31. <https://doi.org/10.1016/j.joms.2017.11.041>.

[28] Azarnoosh J, Sreenivas K, Arabshahi A. Numerical Simulation of Tidal Breathing Through the Human Respiratory Tract. *J Biomech Eng* 2020;142. <https://doi.org/10.1115/1.4046005>.

[29] Collier GJ, Kim M, Chung Y, Wild JM. 3D phase contrast MRI in models of human airways: Validation of computational fluid dynamics simulations of steady inspiratory flow. *J Magn Reson Imaging* 2018;48:1400–9. <https://doi.org/10.1002/jmri.26039>.